Supporting Materials

Text S1 Influence of Co/Fe atomic molar ratio on BPA removal efficiency

As demonstrated in Fig. S2, after adding Co, the removal rate of BPA was remarkably enhanced from 57.4% for Co/Fe-0 to 98.2% for Co/Fe-3% after 30 min of reaction. This improvement indicated that upon increasing the Co doping ratio, the reactive sites on the catalyst surface increased, which increased the contact probability between the catalyst and PMS. The formation of Co^{2+}/Co^{3+} and Fe^{2+}/Fe^{3+} metal ion cyclic pairs and the synergistic effect of bimetals in the reaction system improved the removal rate of BPA. In contrast, when the Co/Fe molar ratio was increased to 4% and 5%, the removal rate of BPA was almost unchanged or even decreased, possibly due to the relatively low BET surface areas of the material. Therefore, the optimal Co/Fe molar ratio of 3% was adopted in this work.

Text S2 Evaluating methods

S2.1 analytical methods

In a typical experiment, 100 mL of BPA solution with an initial concentration of 10 mg/L was taken in a beaker. Then, a quantitative amount of catalyst was added to the beaker and stirred for 30 min to reach adsorption-desorption equilibrium. Next, a predetermined concentration of PMS was added to the beaker to stimulate the degradation reaction. At regular intervals, a certain amount of sample was withdrawn with a pipette and filtered promptly. The obtained samples were immediately quenched with excess MeOH. In addition, the effects of different process parameters were evaluated by varying the experimental parameters (i.e., catalyst dosage, PMS concentration, initial pH, etc.) within the specified range. Finally, the effect of aqueous substrates (Cl^-, NO_3^-, HCO_3^-, SO_4^{2-}, and HA) on BPA removal was investigated. All experiments were performed in triplicate.

S2.2 HPLC analysis

The BPA concentration before and after the reaction was measured using a high-performance liquid chromatography system (HPLC, Shimadzu, LC-2030, Japan) with a reversed-phase InertSustain C18 column (5 μm, 4.6 × 250 mm) and UV detector (λ = 227 nm). The mobile phase was acetonitrile and UP water (55/45; v/v), and the flow rate was 1.0 mL/min. The column temperature was 35℃, and the injection volume was controlled at 20 μL. The degradation rate of BPA was calculated by (Eq. (S1)).

$$R_t = \frac{C_0 - C_t}{C_0} \times 100\% \quad , \quad \text{(S1)}$$

where R_t is the degradation rate, C_0 is the concentration before the reaction, and C_t is the concentration of BPA solution corresponding to the reaction at time *t*.

S2.3 Identification test of main active species

Different quenching agents (methanol, benzoquinone, *tert*-butanol, furfuryl alcohol) were used to examine the active species in the Co-γ-Fe_2O_3/MoS_2/PMS system. Where methanol (MeOH) was used to quench both $SO_4^{\bullet-}$ and •OH, *para*-benzoquinone (*p*-BQ) was selected to scavenge $O_2^{\bullet-}$, *tert*-butanol (TBA) was applied to scavenge •OH, and furfuryl alcohol (FFA) was selected as an $^1O_2$ scavenger. Additionally, the active species were tested via electron paramagnetic resonance (EPR, EMX-PLUS), and •OH, $SO_4^{\bullet-}$, and $^1O_2$ were captured by DMPO and TEMP. The contribution of relevant reactive oxygen species (ROSs) was calculated according to the following (Eqs. (S2)–(S5))

$$R_{\cdot OH} = \frac{k_{\cdot OH}}{k} \approx \frac{(k - k_{TBA})}{k} \quad , \quad \text{(S2)}$$

$$R_{SO_4^{\bullet-}} = \frac{k_{SO_4^{\bullet-}}}{k} \approx \frac{(k_{TBA} - k_{MeOH})}{k} \quad , \quad \text{(S3)}$$

$$R_{^1O_2} = \frac{k_{^1O_2}}{k} \approx \frac{(k_{TBA} - k_{FFA})}{k} \quad , \quad \text{(S4)}$$

$$R_{O_2^{\bullet-}} = \frac{k_{O_2^{\bullet-}}}{k} \approx \frac{(k - k_{p-BQ})}{k} \quad , \quad \text{(S5)}$$

where *R* is the contribution rate corresponding to each ROS (e.g., •OH, $^1O_2$, $O_2^{\bullet-}$, $SO_4^{\bullet-}$), *k* is the reaction rate constant of BPA degradation in the reaction system without an added quenching agent, and k_i is the reaction rate constant of BPA degradation in the reaction system after adding different quenching agents, respectively.

S2.4 Reusability of catalyst

To analyze the reusability of the CO-γ-Fe_2O_3 and Co-γ-Fe_2O_3/MoS_2, five cycles were performed for each experiment. Briefly, the catalyst was separated by permanent magnets after each catalytic degradation experiment, then washed several times with distilled water and used for the next cycle after being dried.

S2.5 Determination of intermediate compounds

Moreover, the intermediates in the degradation of BPA were detected by an LC-MS (Thermo, G6520B, USA). The column and mobile phase were the same as those used in the HPLC section above.

S2.6 Toxicity evaluation

Quantitative structure-activity relationship (QSAR) analysis was performed using Toxicity Estimation Software Tool (T.E.S.T), and bioaccumulation factors, qualitative mutations, and acute and developmental toxicity were analyzed. These four ecotoxicity indicators were used to evaluate the toxicity of the target contaminants and corresponding intermediate products.

Table S1 The removal efficiency of BPA for reported studies by advanced oxidation technologies.

Catalyst	Oxidizing species (agents)	BPA concentration	Removal efficiency	Reference
CuO	PDS	10 mg/L	96% (150 min)	(Sun et al., 2022)
PTh-BiOBr	Light	10 mg/L	83% (100 min)	(Wu et al., 2021)
$BiOI/Mo_2BiO_6$	Light	8 mg/L	90% (300 min)	(Núñez et al., 2023)
Ag-decorated S-doped g $-C_3N_4$	Light	10 mg/L	95% (240 min)	(Oh et al., 2018)
WO_3@MoS_2/Ag	PMS	10 mg/L	92.51% (140 min)	(Zeng et al., 2019)
Co-γ-Fe_2O_3/MoS_2	PMS	10 mg/L	99.3% (10 min)	This work

Table S2 The reaction intermediates to degradation of BPA.

Compound	Retention time (min)	m/z	Chemical formula	Chemical Structure
BPA	6.68	227	$C_{15}H_{15}O_2$	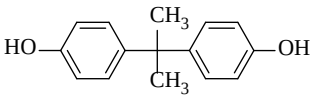
P1	6.14	243	$C_{15}H_{16}O_3$	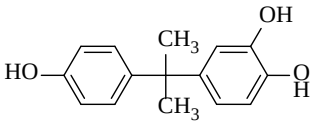
P2	5.95	241	$C_{15}H_{14}O_3$	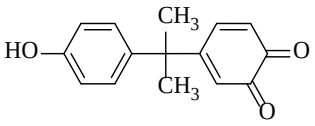
P3	5.09	195	$C_{10}H_{12}O_4$	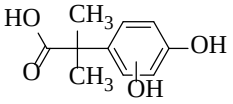
P4	2.70	195	$C_{10}H_{12}O_4$	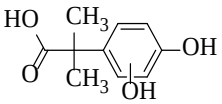
P5	2.40	195	$C_{10}H_{12}O_4$	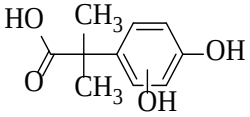
P6	8.51	134	$C_9H_{10}O$	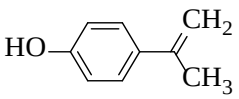
P7	8.75	175	$C_{12}H_{15}O$	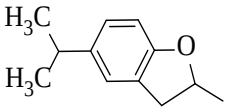
P8	12.24	453	$C_{30}H_{30}O_4$	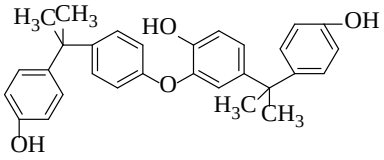
P9	9.07	296	$C_{19}H_{20}O_3$	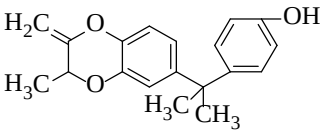
P10	1.08	110	$C_6H_6O_2$	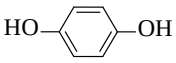

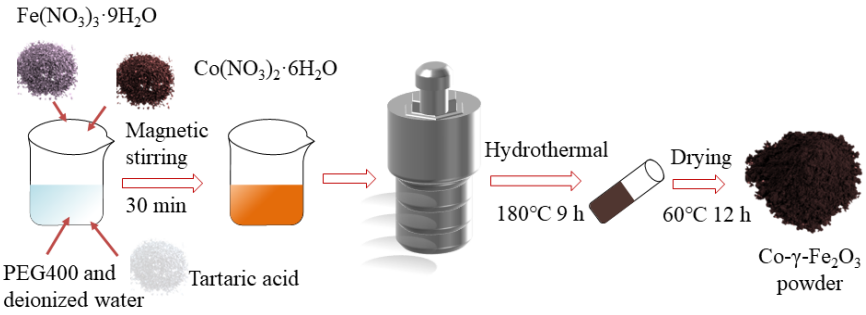

Fig. S1 Schematic diagram of the synthesis of Co-doped γ-Fe_2O_3 Nanostructures.

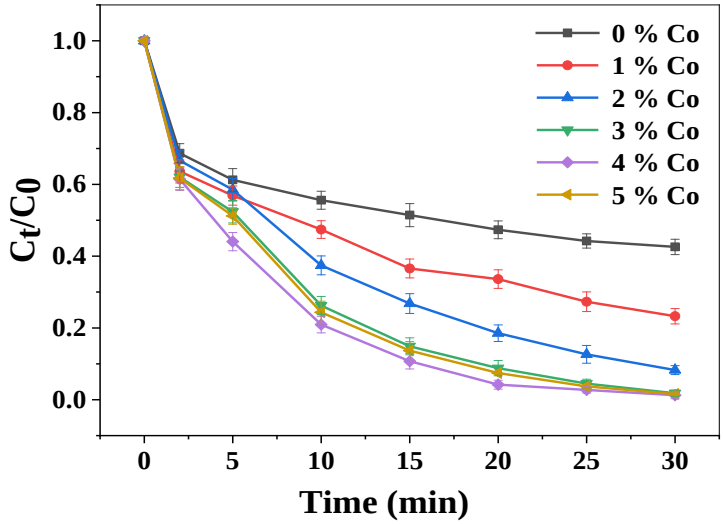

Fig. S2 Effect of Co-γ-Fe_2O_3 with different Co-doping ratios on the removal of BPA.

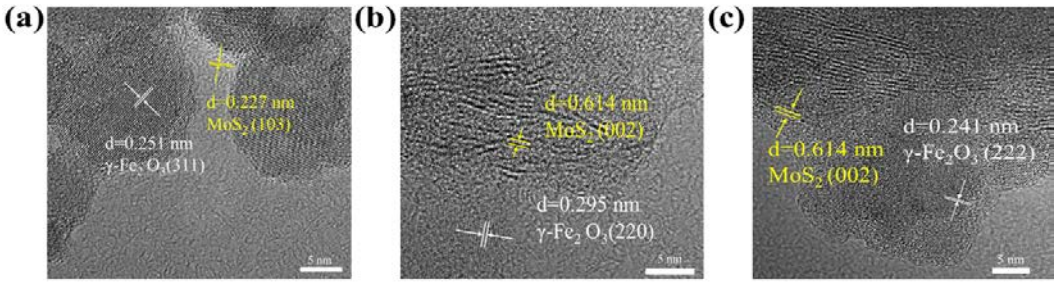

Fig. S3 (a–c) HRTEM images of Co-γ-Fe_2O_3/MoS_2.

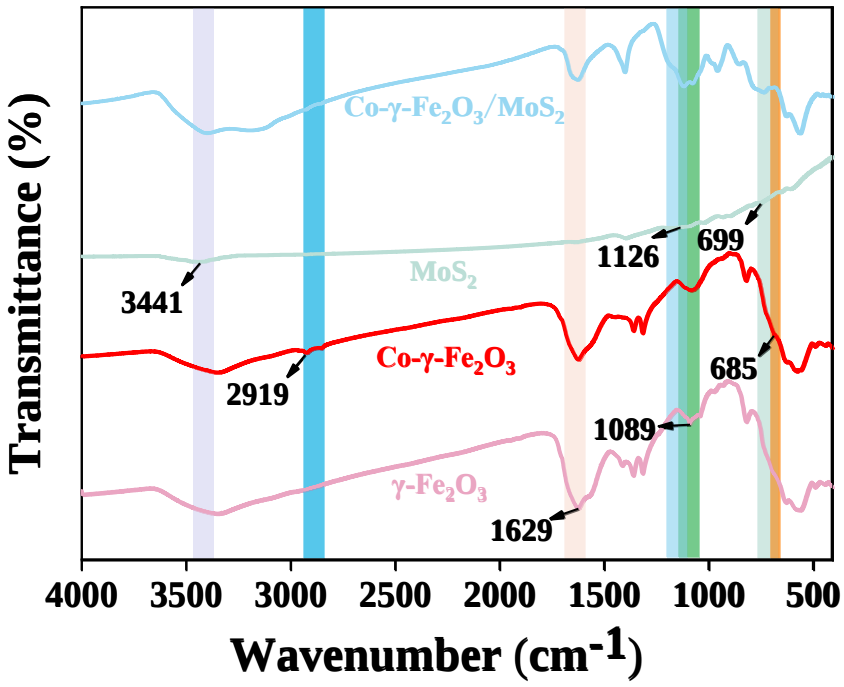

Fig. S4 FTIR spectra of γ-Fe_2O_3, Co-γ-Fe_2O_3, MoS_2 and Co-γ-Fe_2O_3/MoS_2.

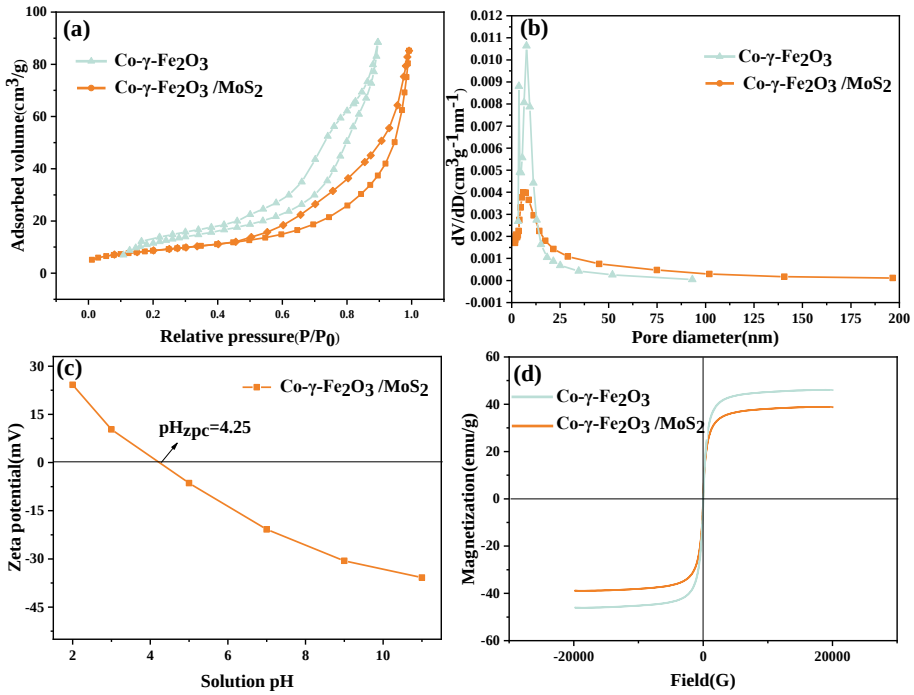

Fig. S5 (a) N_2 adsorption-desorption isotherms; (b) Pore size distribution; (c) Surface zeta potential; (d) Magnetic hysteresis loops of Co-γ-Fe_2O_3 and Co-γ-Fe_2O_3/MoS_2.

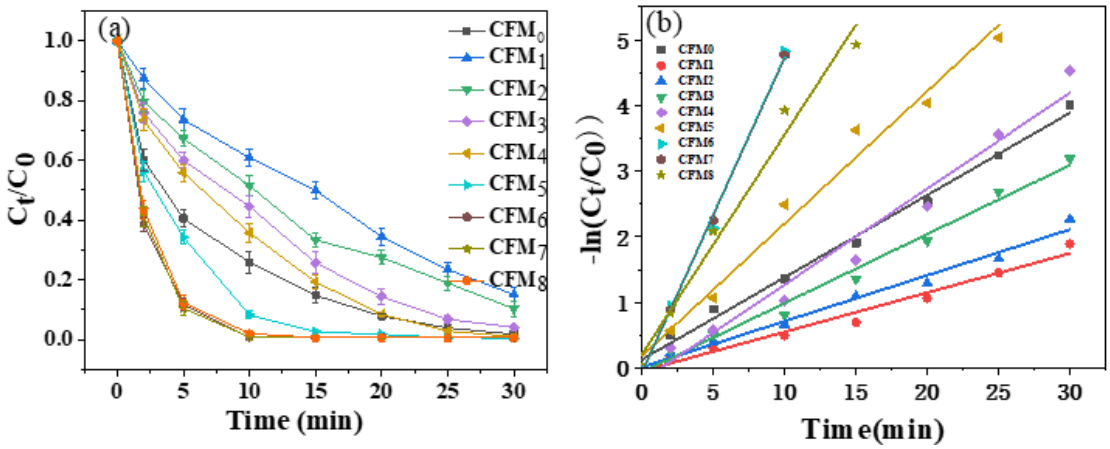

Fig. S6 (a) Removal efficiency of BPA by different catalysts, (b) the corresponding reaction constant; Experimental conditions: $[BPA]_0$ = 10 mg/L, $[Catalyst]_0$ = 0.15 g/L, $[PMS]_0$ = 0.5 mmol/L, pH_0 = 6.30.

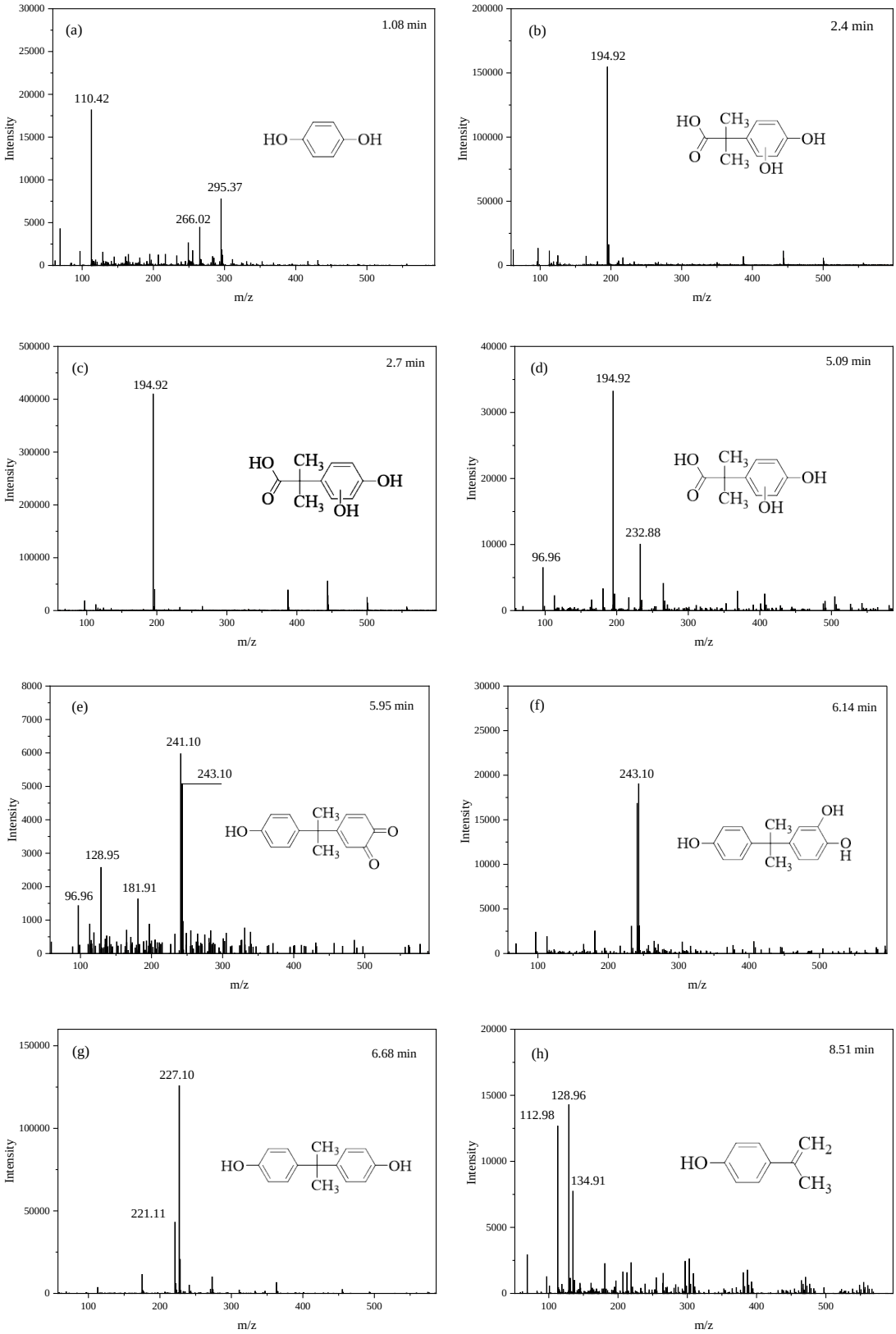
(a)
1.08 min
110.42
295.37
266.02
HO
OH
(b)
2.4 min
194.92
HO
CH3
O
CH3
OH
OH
(c)
2.7 min
194.92
HO
CH3
O
CH3
OH
OH
(d)
5.09 min
194.92
232.88
96.96
HO
CH3
O
CH3
OH
OH
(e)
5.95 min
241.10
243.10
128.95
96.96
181.91
HO
CH3
CH3
O
O
(f)
6.14 min
243.10
HO
CH3
CH3
OH
O
H
(g)
6.68 min
227.10
221.11
HO
CH3
CH3
OH
(h)
8.51 min
128.96
112.98
134.91
HO
CH2
CH3
Intensity
m/z

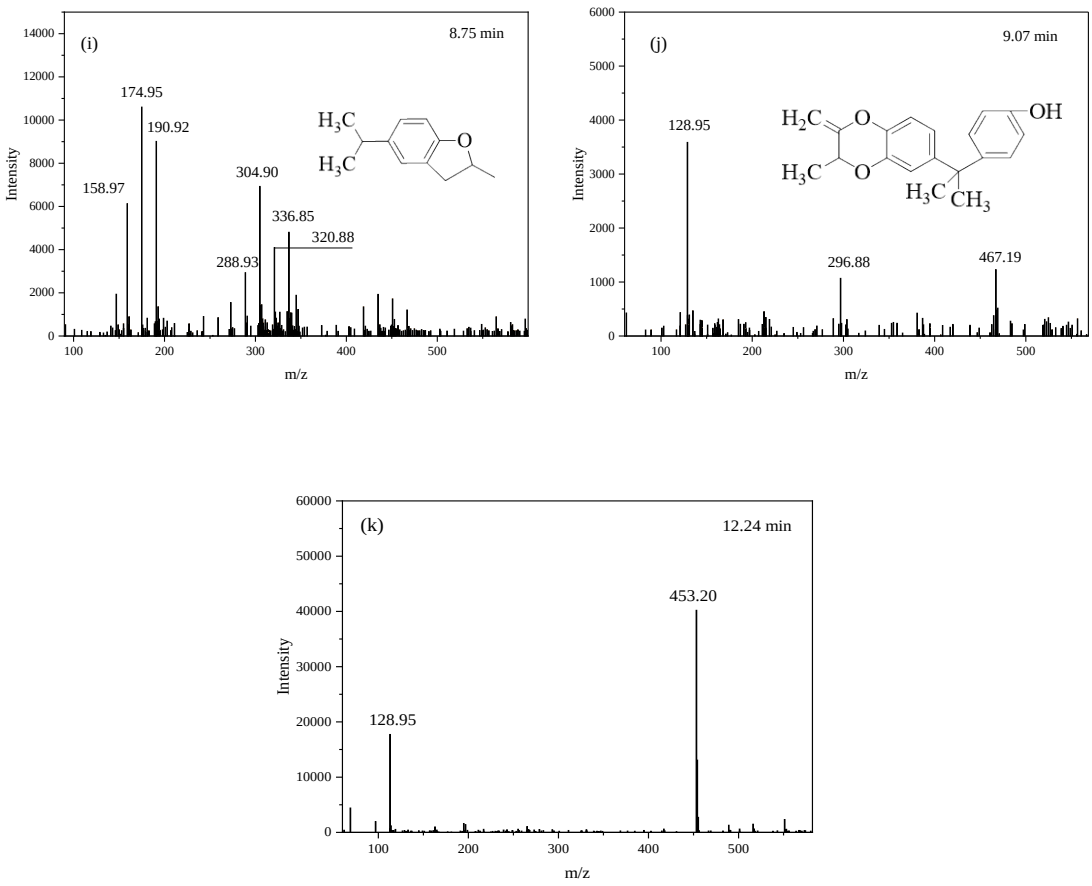

Fig. S7 LC-MS spectrums of BPA and its intermediates. (a) t = 1.08 min, m/z = 110.42; (b) t = 2.40 min, m/z = 194.92; (c) t = 2.70 min, m/z = 194.92;(d) t = 5.09 min, m/z = 194.92; (e) t = 5.95 min, m/z = 241.08; (f) t = 6.14 min, m/z = 243.10; (g) t = 6.68 min, m/z = 227.10; (h) t = 8.51 min, m/z = 134.91; (i) t = 8.75 min, m/z = 174.95; (j) t = 9.07 min, m/z = 296.88;(k) t =12.24 min, m/z = 453.20.

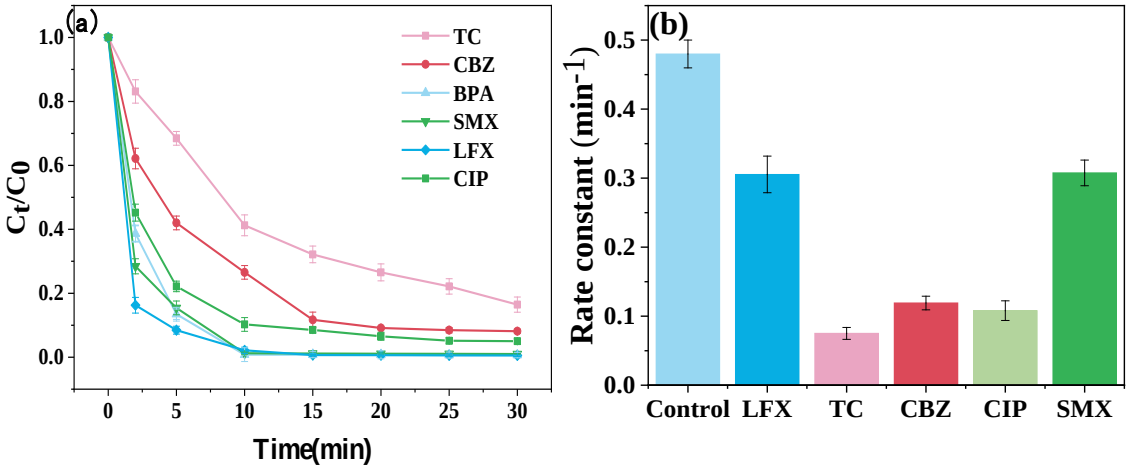

Fig. S8 (a) The removal of various contaminants by Co-γ-Fe_2O_3/MoS_2 process, (b) the corresponding rate constant.

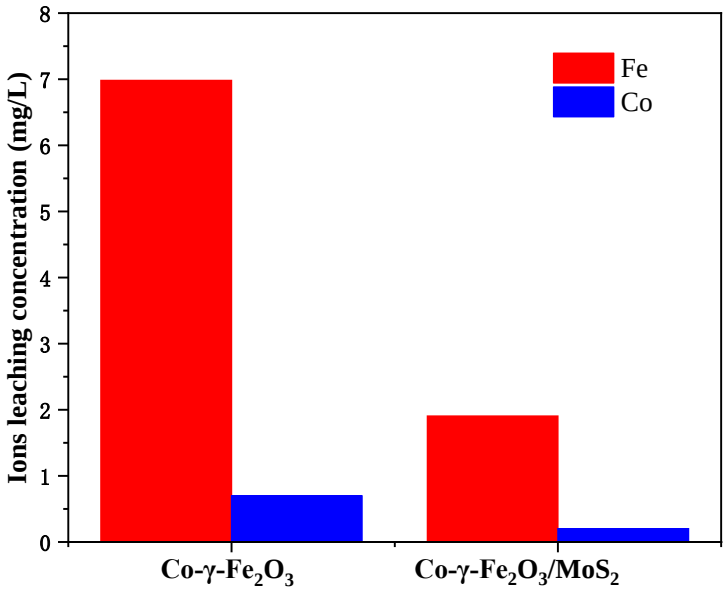

Fig. S9 Fe and Co leaching concentration in the Co-γ-Fe_2O_3/PMS and Co-γ-Fe_2O_3/MoS_2/PMS system, respectively.

References

Núñez M Y N, Rehlaender M Á, Martínez-de La Cruz A, Susarrey-Arce A, Cuevas-Muñiz F M, Sánchez-Domínguez M, Lara-Ceniceros T E, Bonilla-Cruz J, Zapata A A, Hurtado P C, Pérez-Rodríguez M, Orozco A R, González L T, Longoria-Rodríguez F E (2023). Enhancing visible light photocatalytic degradation of bisphenol A using BiOI/Bi2MoO6 heterostructures. Nanomaterials (Basel, Switzerland), 13(9): 1503

Oh W, Lok L, Veksha A, Giannis A, Lim T (2018). Enhanced photocatalytic degradation of bisphenol A with Ag-decorated S-doped g-C3N4 under solar irradiation: Performance and mechanistic studies. Chemical Engineering Journal, 333: 739–749

Sun Z, Zhu Y, Deng Y, Liu F, Ruan W, Xie L, Beadham I (2022). Nature of surface active centers in activation of peroxydisulfate by CuO for degradation of BPA with non-radical pathway. Colloids and Surfaces. A, Physicochemical and Engineering Aspects, 643: 128731

Wu H, Zhou P, Kumar Alagarasan J, Jing J, Zhou T, Xu Y (2021). Construction of novel PTh-BiOBr composite with enhanced photocatalytic degradation of bisphenol A. Advanced Powder Technology, 32(7): 2390–2397

Zeng Y, Guo N, Xu X, Yu Y, Wang Q, Wang N, Han X, Yu H (2019). Degradation of bisphenol A using peroxymonosulfate activated by WO3@MoS2/Ag hollow nanotubes photocatalyst. Chemosphere, 227: 589–597